Power transfer efficiency for obstructed wireless links using Bessel beams

Ravel Pimenta, Gabriel Soriano, Konstantinos Paschaloudis, Mauro Ettorre, Myriam Zerrad, Claude Amra

Research Article | Vol. 31, No. 22 / 23 Oct 2023 / Optics Express 35493
Optics EXPRESS

Power transfer efficiency for obstructed wireless links using Bessel beams

RAVEL C. M. PIMENTA,[1,*] GABRIEL SORIANO,[1] KONSTANTINOS D. PASCHALOUDIS,[2] MAURO ETTORRE,[2] MYRIAM ZERRAD,[1] AND CLAUDE AMRA[1]

[1]Aix Marseille Univ, CNRS, Centrale Méditerranée, Institut Fresnel, Marseille, France
[2]Univ Rennes, CNRS, IETR (Institut d'Électronique et des Technologies du numéRique)-UMR 6164, F-35000 Rennes, France
[*]pimenta@fresnel.fr

Abstract: The power transfer efficiency of a partially obstructed wireless link operating in the Fresnel region is studied in this work. The wireless link consists of two equal apertures, axially aligned, radiating weakly-diffractive beams (truncated Bessel beams). A metallic obstacle is considered along the propagation path of the radiated beam to analyze its impact on the power transfer efficiency with respect to a clear line of sight link. The power transfer efficiency in the obstructed case is derived by resorting to a scattered field formulation. In the proposed approach, the distance between the apertures is considered larger than their radius, which is also bigger than the operating wavelength. A paraxial approximation is then applied to the formulation. Numerical results validate the proposed approach. It appears that the transverse propagation constant of the Bessel Beam and resulting non-diffractive range strongly affects the distance of operation of the wireless link in both the clear and obstructed cases. In addition, we observe how the self-healing property of Bessel beams preserves the efficiency of the partially obstructed link by establishing a resilient link under defined conditions for the propagating beam and size of the obstruction.

1. Introduction

Bessel beams [1] are electromagnetic beams known for their unique property of not experiencing electromagnetic diffraction. These beams are exact solutions to the Helmholtz equation and are characterized by Bessel functions. They also possess the remarkable ability to self-reconstruct their initial intensity profile after propagating around obstacles [2–4]. In [5], the authors employ a wave-optics framework to explain this ability, also known as self-healing. They ultimately conclude that it can be explained in terms of the propagation of plane waves with radial wave vectors situated on a ring. The literature also contains quantitative descriptions of the self-healing property [4,6], as well as studies of non-diffractive beams encountering non-opaque obstacles [7].

These ideal Bessel beams require infinite power and infinite apertures [8], however, in practical applications, Bessel beams are generated with finite radiating apertures and power. Annular slits, axicons, metasurfaces, and hologram are among the technologies used to generate Bessel beams [9]. Some examples of the generation of Bessel Beams are presented in [10–16]. Bessel beams have a wide range of applications, such as optical trapping, material processing, and optical coherence tomography [17]. Also, their potential in wireless communications is particularly promising. With the increasing demand for faster and more reliable networks [18], wireless communication systems are transitioning to millimeter waves with larger operating bands. However, this transition comes at the cost of increased propagation losses [19], primarily due to electromagnetic diffraction [20]. In the light of this, Bessel beams offer are an attractive solution for enhancing wireless communication systems.

#499123 https://doi.org/10.1364/OE.499123
Journal © 2023 Received 27 Jun 2023; revised 18 Sep 2023; accepted 22 Sep 2023; published 9 Oct 2023

Optics EXPRESS

This paper focuses on the effect of truncation on Bessel beams. A key aspect of truncated Bessel beams is the existence of a non-diffractive range (NDR) [20,21], which delineates two distinct regions. Within the NDR, the truncated beams slightly spread while propagating, preserving their field profile as compared to other kinds of beams such as Gaussian beams [22]. However, beyond the NDR, Bessel beams undergo diffraction. Notably, the NDR falls within the Fresnel region [23], implying that the link budget of a wireless link cannot be directly derived using the Friis formula typically applied for far-field links [19].

In this study we are interested in deriving the power transfer efficiency of a partially obstructed wireless link, expressed as the ratio between the accepted power at the receiving side and the available power at the transmitter. Previous works in literature considered the link budget for wireless links using truncated Bessel beams without obstructions [22,24–26]. The contribution of this paper is to extend the wireless power transfer efficiency (WPTE) formulation [22,27,28] to partially obstructed wireless links, in order to develop a model that can predict the impact of the size and position of an obstruction on the efficiency of the link.

The direct application of the WPTE formulation requires the calculation of the electric and magnetic fields between the radiating apertures for a given excitation [27]. We will consider two planar axially aligned radiating apertures as in [28]. This approach is followed in [22] and leads to a very complete study of the WPTE for apertures radiating cylindrical Bessel beam. More recently, in [24], the radiating apertures are assumed to be cut in infinite ground planes affecting the overall link budget. In particular, the two ground planes behave as a parallel-plate waveguide (PPW) environment [29] with the appearance of resonances due to mode traveling within the PPW. In this paper, we focus on the WPTE between apertures at distances much larger than their size. In such a configuration, considering a PPW environment appears irrelevant, and the approach by [22,28] is preferred. In addition, in [22], it is shown that radially polarized Bessel beams outperform radially polarized Gaussian beams for WPTE in the Fresnel region.

This work focuses on utilizing large apertures of radii equal to or larger than 50λ, where λ is the free space wavelength at the operating frequency. The purpose is to create a wireless link operating at distances larger than 4000λ, which is more than 40 times the apertures' size, fully justifying the use of the paraxial approximation [22] for the formulation. In the following, radially polarized transverse magnetic (TM) fields will be considered over the radiating apertures. However, other field distributions may be considered without affecting the overall approach and general conclusions of the work.

The paper is structured as follows. In Section 2, the WPTE formula is provided and analyzed and then extended to the obstructed case. Next, in Section 3, the TM radially polarized and truncated Bessel beams are detailed. Also in this section, the formulation is first validated and then used to perform a thorough study of an obstructed wireless link from a power transfer efficiency point of view. We chose an axially aligned Perfect electric conductor (PEC) disk as a canonical scatterer. The conclusions with the most salient and counterintuitive results are presented in section 4.

2. Wireless power transfer efficiency

2.1. Clear line of sight

The WPTE for a general system of two conjugately matched lossless antennas, in a time-harmonic regime, was first derived in [27]. For two antennas, a and b, the WPTE formula is given by [22,28]:

$$\Gamma = \frac{|\langle a, b\rangle|^2}{16 P_a P_b} \tag{1}$$

where $P_{a(b)}$ is the total power radiated by antenna $a(b)$ when antenna $a(b)$ is emitting while antenna $b(a)$ is receiving, and $\langle a, b\rangle$ is the so-called electromagnetic reaction [30] between

Optics EXPRESS

antennas a and b. Throughout this paper, the time-harmonic dependence $e^{-i\omega t}$, where ω is the angular frequency, is assumed and suppressed.

The system we analyze in this paper is shown in Fig. 1. A cylindrical coordinate system (ρ, ϕ, z) is adopted to describe the geometry of the problem. The TX (aperture a) and RX (aperture b) are two identical circular radiating apertures, facing each other and axially aligned, located respectively at $z = 0$ and $z = L$. TX and RX can be considered radiating apertures supporting a single operating mode [31]. In particular, we consider a radially polarized TM mode with respect to z (TM_z) [29]. Therefore, the transverse components are $E_\rho(\rho, z)$ and $H_\phi(\rho, z)$.

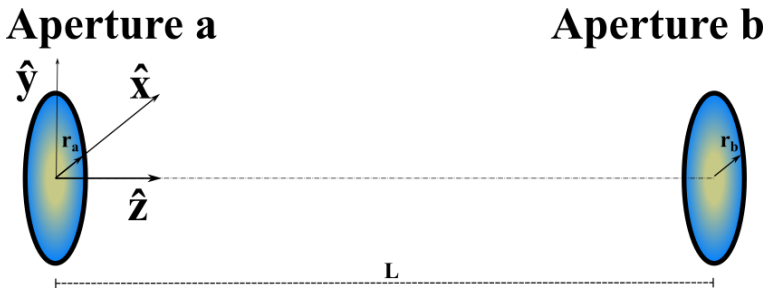

Fig. 1. Schematic view of the wireless link without obstruction.

The modes in both apertures are described by a common mode function $K(\rho)$ and complex scalars $V_{a(b)}$ and $I_{a(b)}$. The mode function $K(\rho)$ is real-valued, limited by the radius $r_a = r_b$ of the apertures : $K(\rho{>}r_a) = 0$, and writes as an Hankel transform [32], yielding:

$$K(\rho) = \int_0^\infty \tilde{K}(k_\rho) J_1(k_\rho \rho)\, k_\rho\, dk_\rho \tag{2}$$

where k_ρ is the spectral variable, and $K(\rho)$ is furthermore normalized as:

$$2\pi \int_0^{r_a} K^2(\rho)\, \rho\, d\rho = 2\pi \int_0^\infty |\tilde{K}(k_\rho)|^2\, k_\rho\, dk_\rho = 1 \tag{3}$$

The electric field in both excitation conditions, assuming a complete non-reflection condition at $z = 0^+$ and $z = L^-$ can be written as:

$$E_\rho^a(\rho, z) = V_a \int_0^\infty e^{ik_z z} \tilde{K}(k_\rho) J_1(k_\rho \rho)\, k_\rho\, dk_\rho \tag{4}$$

for a emitting while b is receiving, and for the reciprocal excitation where b is emitting while a is receiving, as:

$$E_\rho^b(\rho, z) = V_b \int_0^\infty e^{ik_z (L-z)} \tilde{K}(k_\rho) J_1(k_\rho \rho)\, k_\rho\, dk_\rho \tag{5}$$

k_z is derived from the wavenumber in vacuum $k_0 = \omega/c$ by:

$$k_z = \begin{cases} \sqrt{k_0^2 - k_\rho^2} & k_\rho{<}k_0 \\ i\sqrt{k_\rho^2 - k_0^2} & k_\rho{>}k_0 \end{cases} \tag{6}$$

The magnetic fields are derived considering the wave admittance as the intrinsic admittance of vacuum Y_0. This paraxial approximation can be justified by two arguments. First, the distance L

Optics EXPRESS

between the apertures is much larger than their radius r. Second, r is assumed much larger than the wavelength in vacuum, $\lambda = 2\pi/k_0$. The magnetic fields thus write:

$$H_\phi^a(\rho, z) = Y_0 V_a \int_0^\infty e^{ik_z z} \tilde{K}(k_\rho) J_1(k_\rho \rho)\, k_\rho\, dk_\rho \tag{7}$$

$$H_\phi^b(\rho, z) = -Y_0 V_b \int_0^\infty e^{ik_z (L-z)} \tilde{K}(k_\rho) J_1(k_\rho \rho)\, k_\rho\, dk_\rho \tag{8}$$

Total power P_a and P_b of formula (1) are thus:

$$P_a = \pi Y_0 |V_a|^2 \Re e \int_0^\infty |\tilde{K}(k_\rho)|^2\, k_\rho\, dk_\rho \tag{9}$$

$$P_b = \pi Y_0 |V_b|^2 \Re e \int_0^\infty |\tilde{K}(k_\rho)|^2\, k_\rho\, dk_\rho \tag{10}$$

while the reaction writes, using the generalized reciprocity theorem [27] on any plane of abscissa z for $0 \le z \le L$:

$$\langle a, b \rangle = 4\pi Y_0 V_a V_b \int_0^\infty e^{ik_z L} |\tilde{K}(k_\rho)|^2\, k_\rho\, dk_\rho \tag{11}$$

finally leading to the WPTE expression:

$$\Gamma = \frac{\left| \int_0^\infty e^{ik_z L} |\tilde{K}(k_\rho)|^2\, k_\rho\, dk_\rho \right|^2}{\left(\Re e \left[\int_0^\infty |\tilde{K}(k_\rho)|^2\, k_\rho\, dk_\rho \right] \right)^2} \tag{12}$$

2.2. Obstructed links

The formulation presented in section 2.1 was derived for systems operating in clear line of sight (CLOS). However, in a real case scenario, an obstacle may appear in the propagation path, and so it is interesting to extend this formulation to obstructed links, as shown in Fig. 2.

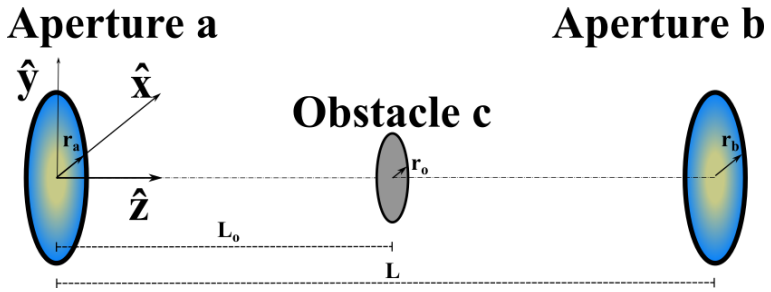

Fig. 2. Schematic view of a wireless link with a metallic obstruction. The obstruction has a radius r_o, zero thickness, and is placed at $z = L_o$

To proceed with this formulation, we recall that the reaction is a linear operation. Therefore, if we have three sources (a, b and c) radiating in the same region and at the same frequency [30], the reaction term will be:

$$\langle (a + c), b \rangle = \langle a, b \rangle + \langle c, b \rangle \tag{13}$$

where a, b and c represent the emitter, the receiver and the obstacle, respectively. In this case, the source c is created due to the fields radiated by a, generating currents over c radiating the scattered fields $\vec{E}_a^s$ and $\vec{H}_a^s$. If b is acting as the emitter, c is dependent on b and it radiates the

Optics EXPRESS

scattered fields $\vec{E}_b^s$ and $\vec{H}_b^s$. We also define the incident fields as the ones radiating from the apertures without the obstacle. Thus, if a is the emitter, the incident fields are $\vec{E}_a^i$ and $\vec{H}_a^i$, while if b is emitting, the incident fields are $\vec{E}_b^i$ and $\vec{H}_b^i$.

We replace the obstacle by a the current distribution on its surface, named source c (scattered source). We also define the total reaction, $\langle a, b\rangle_T$, as the reaction of a and b with the scattered source c present. The total reaction is composed by two terms, the incident reaction and the scattered reaction [33], and it can be written as:

$$\langle a, b\rangle_T = \langle a, b\rangle^i + \langle a, b\rangle^s = \langle a, b\rangle^i + \langle c, b\rangle \tag{14}$$

$$\langle a, b\rangle^i = \int \vec{E}_a^i(\vec{r}) \cdot \vec{J}_b^i(\vec{r}) - \vec{H}_a^i(\vec{r}) \cdot \vec{M}_b^i(\vec{r})\, d\vec{r} \tag{15}$$

$$\langle a, b\rangle^s = \int \vec{E}_a^s(\vec{r}) \cdot \vec{J}_b^i(\vec{r}) - \vec{H}_a^s(\vec{r}) \cdot \vec{M}_b^i(\vec{r})\, d\vec{r} = \int \vec{E}_b^i(\vec{r}) \cdot \vec{J}_c(\vec{r}) - \vec{H}_b^i(\vec{r}) \cdot \vec{M}_c(\vec{r})\, d\vec{r} \tag{16}$$

where $\langle a, b\rangle^i$ represents the reaction of the incident components, $\langle a, b\rangle^s$ the reaction of the scattered components. $\vec{M}_b^i$ and $\vec{J}_b^i$ represent the magnetic and electric current on the source b, respectively, when b is emitting without the obstacle. Furthermore, $\vec{J}_c(\vec{M}_c)$ is the electric(magnetic) current on the surface of the obstacle. The expression on the right side of Eq. (16) is obtained using the reciprocity theorem [23]. Finally, we can use Eq. (14) to extend Eq. (1) to the obstructed case:

$$\Gamma = \frac{|\langle a, b\rangle^i + \langle a, b\rangle^s|^2}{16 P_a P_b} \tag{17}$$

The incident reaction can be easily calculated, as discussed in Subsection 2.1. The scattered reaction can be estimated using an approximation technique, such as the Method of Moments (MOM) [34,35] or Physical Optics (PO) [23,33].

The formulation which we are deriving is focused on perfectly electric conducting (PEC) obstacle. Consequently, Eq. (16) reduces to:

$$\langle a, b\rangle^s = \int_0^{r_o} E_\rho^b(\rho, L_o) \cdot J_\rho^c(\rho) \rho\, d\rho \tag{18}$$

where r_o is the radius of the obstacle, which is placed at $z = L_o$, and $\vec{J}_c$ reduces to its tangential component J_ρ^c. Furthermore, we have the following boundary conditions on the surface of the obstacle [30]:

$$E_\rho^a(\rho, L_o) = -E_\rho^{as}(\rho, L_o) \tag{19}$$

$$E_\rho^b(\rho, L_o) = -E_\rho^{bs}(\rho, L_o) \tag{20}$$

where $E_\rho^{as}(E_\rho^{bs})$ is the scattered tangential electric fields when $a(b)$ is the emitter. Then, using Eq. (20) we can derive:

$$\langle a, b\rangle^s = -\int_0^{r_o} E_\rho^{bs}(\rho, L_o) \cdot J_\rho^c(\rho) \rho\, d\rho \tag{21}$$

To reduce the difference between the correct and the approximated value of $\langle a, b\rangle^s$ due to the estimated current, we propose using a variational approach [29,36]. The variational procedure is used here to obtain a formula that is almost insensitive to relatively small variations around the correct value [29]. This stationary formula, or variational solution, is derived treating the problem as a differential scattering problem [30,33].

We now consider that when a is the emitter, the exact current on the obstacle is defined by c_a and its approximation is g. Similarly, when b is emitting, the exact current on the obstacle is defined by c_b and its approximation by h. These approximated currents must have the same

Optics EXPRESS

self-reaction term as on their respective correct currents [29]. To ensure this condition, we impose:

$$\langle g, h\rangle \approx \langle a, b\rangle_s \tag{22}$$

$$\langle g, h\rangle = \langle c_b, g\rangle = \langle h, c_a\rangle \tag{23}$$

Also, Eq. (23) can be related to the sources a and b if we use Eq. (19) and (20):

$$\langle g, h\rangle = -\langle b, g\rangle = -\langle a, h\rangle \tag{24}$$

$$\langle g, h\rangle\langle g, h\rangle = \langle b, g\rangle\langle a, h\rangle \tag{25}$$

$$\langle a, b\rangle_s \approx \langle g, h\rangle = \frac{\langle b, g\rangle\langle a, h\rangle}{\langle g, h\rangle} \tag{26}$$

The relation expressed in (26) can be combined with Eq. (21) to obtain the stationary formula for $\langle a, b\rangle^s$ [29,30]:

$$\langle a, b\rangle_s \approx \frac{\int_0^{r_o} E^b_\rho(\rho, L_o)\cdot J^g_\rho(\rho)\rho\, d\rho \int_0^{r_o} E^a_\rho(\rho, L_o)\cdot J^h_\rho(\rho)\rho\, d\rho}{\int_0^{r_o} E^h_\rho(\rho, L_o)\cdot J^g_\rho(\rho)\rho\, d\rho} \tag{27}$$

where J^g_ρ is electric current of g and J^h_ρ is the one due to the source h. Furthermore, E^h_ρ is the free-space field radiated by $J^h_\rho(\rho)$. To calculate the WPTE for obstructed links, we need to calculate the reaction of the scattered components, $\langle a, b\rangle^s$, and it can be calculated using Eq. (18) or Eq. (27). We define the WPTE variational solution (VS) as the WPTE solution in which we use Eq. (27) to obtain the scattered reaction. For this solution, J^g_ρ and J^h_ρ, in Eq. (27), are calculated using the the Physical Optics approximation [23]. Additionally, we also define the WPTE Pure PO solution (PPO) as the WPTE solution in which the scattered reaction is calculated using Eq. (18), in which the Physical Optics approximation is used to calculate J^c_ρ.

3. Numerical analysis

3.1. TM_z Bessel beam and NDR

We present, in this section, the numerical results of the obstructed formulation of the WPTE between two apertures radiating radially polarized, TM_z, weakly-diffractive Bessel beams. The mode function $\tilde{K}(k_\rho)$ of a radially polarized Bessel beam can be written as:

$$\tilde{K}(k_\rho) = \frac{A r_a \left[k_\rho J_0(k_\rho r_a) J_1(k_n r_a) - k_n J_0(k_n r_a) J_1(k_\rho r_a)\right]}{k_n^2 - k_\rho^2} \tag{28}$$

$$k_n = \frac{j_{0n}}{r} \tag{29}$$

where A is the normalization factor, r_a is the radius of the aperture, j_{0n} is the n-th zero of the Bessel function of the 0-th order and first kind, $J_0(k_n\rho)$. The function $K(\rho)$ is, then, written as a Hankel Transform using Eq. (2), and $E^a_\rho(\rho, z)$, $E^b_\rho(\rho, z)$, $H^a_\phi(\rho, z)$ and $H^b_\phi(\rho, z)$ can be easily obtained as derived in Subsection 2.1. The NDR is obtained using the radius of the aperture r_a, k_0 and k_n, as shown in Eq. (30). As $j_{0n}<j_{0(n+1)}$, and therefore $k_n<k_{n+1}$, it is clear that for the same aperture radius the largest NDR is achieved when $k_n = k_1$. This indicates that, considering the same aperture size and separation distance, the largest operating range is obtained using k_1.

$$\text{NDR} = r_a\sqrt{\left(\frac{k_0}{k_n}\right)^2 - 1} \tag{30}$$

Figure 3 illustrates the amplitude of the tangential component of two distinct radially polarized TM_z Bessel beams: one with with $k_n = k_1$ and the other with $k_n = k_4$. We observe the Bessel

Optics EXPRESS

beam has one lobe for $k_n = k_1$ and four lobes for $k_n = k_4$. For both cases, we have zero field amplitude along the axis z. The impact of beam truncation becomes apparent when we observe diffraction occurring around the edges of the aperture.

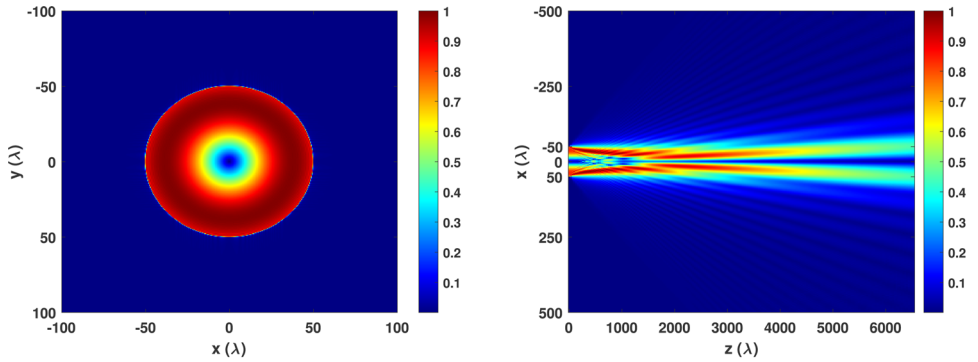

(a) Electric field over the radiating aperture with $k_n = k_1$ (b) Electric field propagating along z ($y = 0$) with $k_n = k_1$

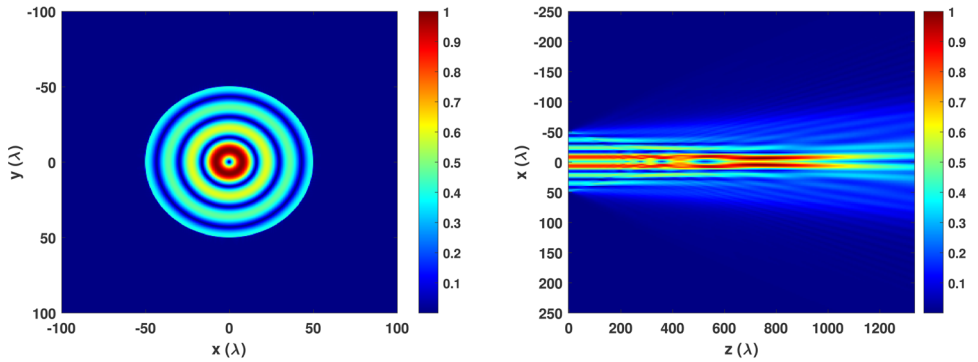

(c) Electric field over the radiating aperture with $k_n = k_4$ (d) Electric field propagating along z ($y = 0$) with $k_n = k_4$

Fig. 3. Normalized amplitude of the tangential component of radially polarized TM_z Bessel Beams with different k_n. The chosen aperture radius is 50λ, and the NDR is 6531λ and 1331λ for kk_1 and k_4, respectively.

On Fig. 4, the wireless power transfer efficiency of an unobstructed link as a function of the separation distance for a TM_z Bessel distribution is presented. The WPTE is calculated using Eq. (1). The aperture radius is set to $r_a = 50\lambda$, $k_n = k_1$ and NDR = 6531λ. We can notice, on Fig. 4, that the NDR marks the limit between two different regimes for the WPTE. For z<NDR, the efficiency decreases almost linearly with the distance, mostly due to the weakly diffractive nature of the beam. For z>NDR, the Bessel beam is more impacted by diffraction and so the link efficiency decreases more rapidly and quadratically.

3.2. *Validation of the approach*

Initially, the PPO and VS solutions are compared, considering equal apertures facing each other. On this comparison, and also for the remaining numerical evaluations, the obstacle is a perfectly electric PEC disk axially aligned to the apertures. The obstacle is placed at $z = 0.2$NDR, its radius, r_o, is 30% of the aperture radii, r_a, and $2\lambda \leq r_a \leq 50\lambda$. For this analysis, we define $\Delta\Gamma$ as the impact of the scattered reaction, $\langle a, b \rangle^s$, on the WPTE. $\Delta\Gamma$ is calculated using Eq. (31).

Optics EXPRESS

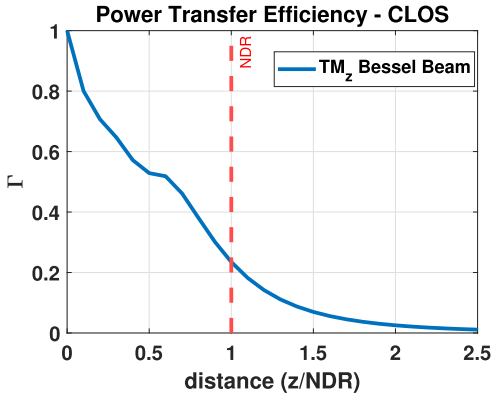

Fig. 4. WPTE as a function of the separation distance. The system operates with CLOS. The red dashed line indicates the NDR limit The used parameters are: $r_a = 50\lambda$, $k_n = k_1$, and NDR = 6531λ.

Figure 5 shows $\Delta\Gamma$ as a function of the separation distance between the apertures.

$$\Delta\Gamma = \frac{|\langle a,b\rangle^i + \langle a,b\rangle^s|^2 - |\langle a,b\rangle^i|^2}{16P_aP_b} \tag{31}$$

On Fig. 5, we can see that when $r_a = 2\lambda$, the PPO and VS results do not closely agree. The maximum relative difference between the two solutions observed is around 70%. As we increase the dimensions of the problem (aperture radius and separation distance) this difference rapidly decreases. For the larger apertures, the maximum relative difference observed do not exceed 3 %. Furthermore, this confirm that single scattering is the dominant mechanism here.

The VS and the full-wave commercial software COMSOL Multiphysics [37] are compared in order to validate the proposed approach. We evaluate the WPTE as a function of the separation distance between the apertures. Furthermore, the distance is normalized by the NDR. For this validation, the radius of aperture a and b are defined as r_a and r_b, respectively, and $r_a = r_b = 4\lambda$. The obstacle is a PEC disk axially aligned to the apertures, its radius is $r_o = 0.3r_a$, $k_1 = 20.04$, and the NDR = 41λ. These parameters were chosen to reduce the computational time without affecting the overall conclusions. The results are presented in Fig. 6 and Fig. 7.

On Fig. 6, the WPTE of an unobstructed link is verified to establish a reference. The numerical results are compared with those of COMSOL. Overall, we observe, in average, small differences of about 0.01. Close to z =NDR, the difference is not greater than 0.02 for an efficiency of 0.25. Fig. 7(a) and 7(b) show the results of the VS formulation and COMSOL for an obstructed link. On Fig. 7(a), the obstacle is placed at $z = 0.1$NDR, while on Fig. 7(b) the obstacle is placed at $z = 0.2$NDR. We can see a close agreement between the results. The differences are smaller than 0.02.

The dimensions of the problem studied are not ideal for the VS formulation developed because, as stated earlier, it assumes that the radii of the apertures is much smaller than the separation distance between the apertures. Therefore we can expect our model to be much more accurate than 0.02 on the efficiency. As a conclusion, this comparison shows that our model is sufficiently accurate in order to quantify the influence of obstructions on the link efficiency.

3.3. Numerical results

In the numerical analysis, $r_a = r_b = 50\lambda$, and r_o assumes three values: $0.1r_a$, $0.2r_a$ and $0.3r_a$. Again, the WPTE is evaluated as a function of the distance. All calculations are performed using

Optics EXPRESS

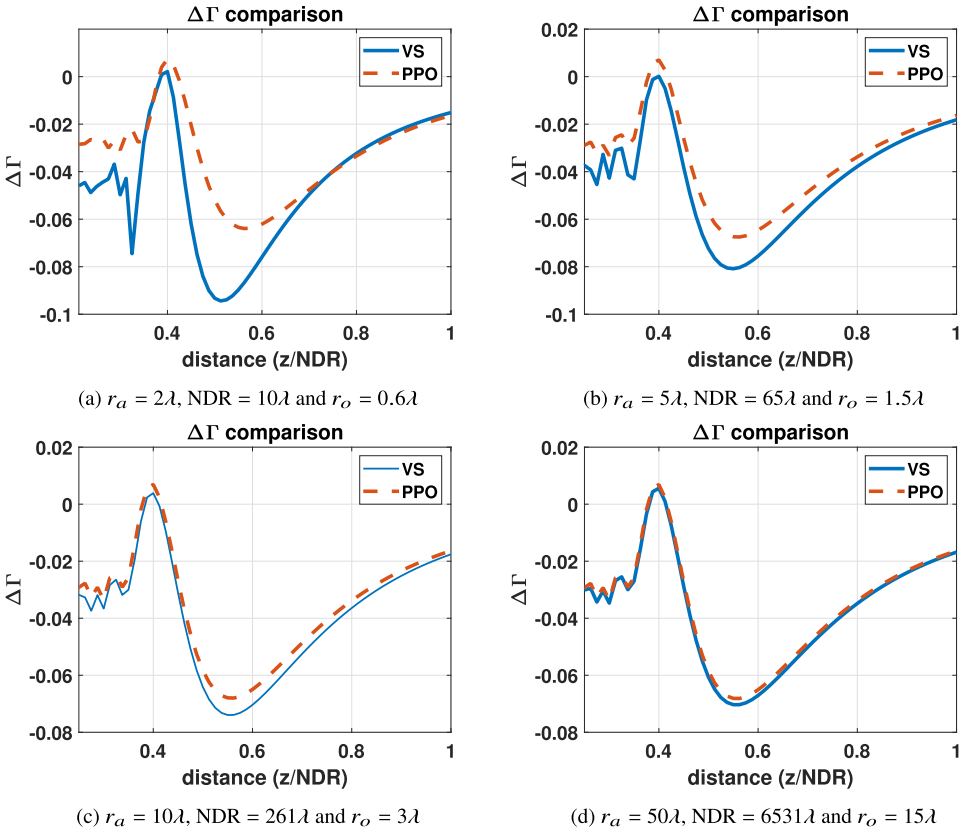

(a) $r_a = 2\lambda$, NDR = 10λ and $r_o = 0.6\lambda$

(b) $r_a = 5\lambda$, NDR = 65λ and $r_o = 1.5\lambda$

(c) $r_a = 10\lambda$, NDR = 261λ and $r_o = 3\lambda$

(d) $r_a = 50\lambda$, NDR = 6531λ and $r_o = 15\lambda$

Fig. 5. $\Delta\Gamma$ of VS and PPO solutions compared as function of the separation distance between the radiating apertures. The used parameters are: $r_o = 0.3r_a$, $k_n = k_1$ and the obstacle is placed at $z = 0.2$NDR.

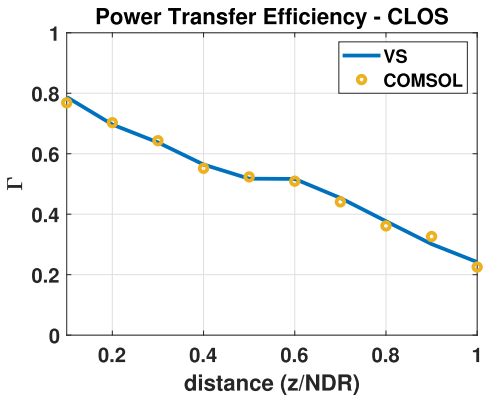

Fig. 6. WPTE as a function of the separation distance. The system operates with CLOS. The blue line shows the results of the numerical calculations and the yellow circles those obtained with COMSOL. The used parameters are: $r_a = 4\lambda$, $k_n = k_1$, and NDR=41λ.

Optics EXPRESS

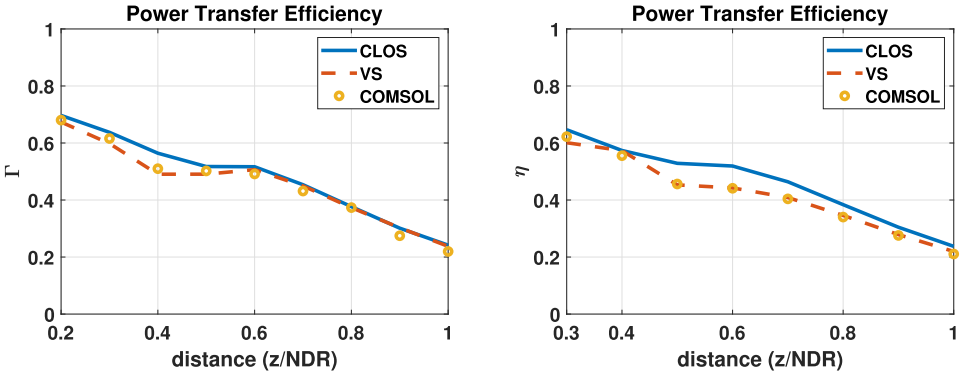

(a) Obstacle placed at $z = 0.1$NDR, $r_o = 0.3r_a$

(b) Obstacle placed at $z = 0.2$NDR, $r_o = 0.3r_a$

Fig. 7. WPTE as a function of the separation distance for obstructed links. The blue line is the WPTE for an unobstructed link, the dashed red line is the numerical calculation of the obstructed link and the circles are numerical results by COMSOL. The used parameters are: $r_a = 4\lambda$, $k_n = k_1$, and NDR=41λ.

the VS solution derived in subsection 2.2. The results of this configuration are shown in Fig. 8, 9 and 10.

Figure 8 shows the WPTE as a function of the separation distance for a partially obstructed link. The obstacle is placed at four different positions along the z axis. The separation distance goes from the obstacle until the NDR (NDR= 6531λ). We can notice that the obstacle of $0.1r_a$ does not disturb the WPTE, regardless of its position. When the obstacle radius is $0.2r_a$, we can see a drop in efficiency and its gradual recovery to the level of the unobstructed link. For an obstacle with a radius equal to $0.3r_a$, we can also see a drop in efficiency and its consequent recovery. However, the efficiency is not fully restored to the level of the unobstructed link. In Fig. 8, the complete (or almost complete) recovery of the efficiency to the level of the unobstructed link constitutes an impressive illustration of the self-healing properties of Bessel Beams. Contra-intuitively, we see that the link efficiency is more disturbed when the obstacle is placed halfway between the two apertures, and not close to the apertures. Therefore, for focused systems [22], we can expect even greater disturbances on the efficiency for obstacles located near the focal point. According to the Geometrical Optics theory, the shadow due to an obstacle, which is the region where the electromagnetic fields are yet not reconstructed, is $s \approx r_o k_0/2k_n$ [2]. However, the results of our wave model do not show a direct relationship between the shadow region and the WPTE.

Figure 9 illustrates the relation between the WPTE the obstacle radius for a given configuration. For this study, we considered $r_a = 50\lambda, k_n = k_1, 0<r_o \leq r_a$, and the obstruction was placed at $z = 0.2$NDR. The WPTE was evaluated at $z = 0.8$NDR in order to evaluate the influence of the obstacle radius on the efficiency for distances within the NDR. We observe that when $r_o \leq 0.2r_a$ the impact of the efficiency is almost negligible. As the obstacle radius increases to the range of $0.2r_a \leq r_o \leq 0.4r_a$, the impact of the obstacle becomes more visible although the efficiency drop is not greater than 0.07 in this region. For obstacles greater than $0.4r_a$, we observe a notable change in the curve's trend, indicating that the link becomes more sensitive to the radius of obstacle. This can be clearly seen as the efficiency drops 0.15 when the radius increases from $0.4r_a$ to $0.6r_a$.

On Fig. 10(a), we verify the impact of k_n on the efficiency of the unobstructed link for a constant aperture radii. The variable k_n is calculated using the first four zeros of $J_0(k_n\rho)$, so $1 \leq n \leq 4$. We have four different Bessel beams with different NDR as imposed by the different transverse propagation constants, k_n (k_1, k_2, k_3 and k_4). Each beam is identified by its k_n. In our

Optics EXPRESS

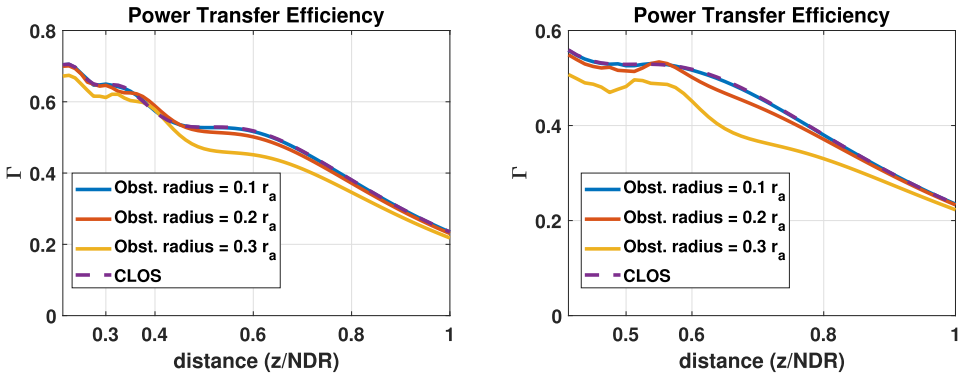

(a) Obstacle placed at $z = 0.2$NDR

(b) Obstacle placed at $z = 0.4$NDR

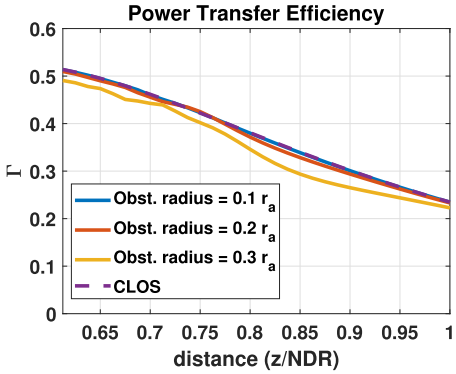

(c) Obstacle placed at $z = 0.6$NDR

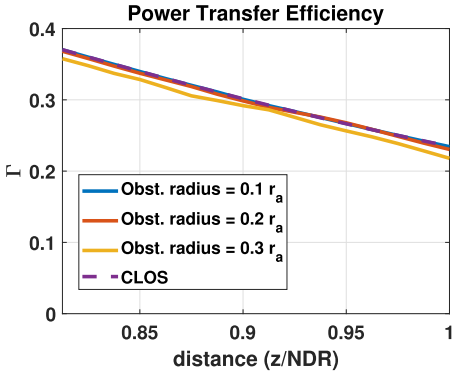

(d) Obstacle placed at $z = 0.8$NDR

Fig. 8. WPTE for obstructed links for different obstacles placed at different locations along z. The WPT is evaluated as a function of the distance. The distance is normalized with respect to the NDR. The dashed line represents the WPTE for the unobstructed link. The used parameters are: $r_a = 50\lambda$, $k_n = k_1$, and NDR $= 6531\lambda$.

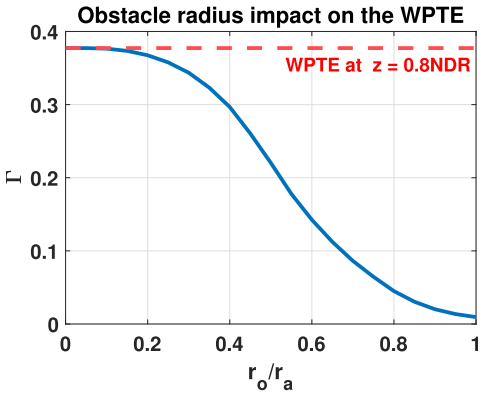

Fig. 9. WPTE as a function of the obstacle radius. The obstacle is placed at $z = 0.2$NDR and the WPTE is evaluated at $z = 0.8$NDR. The dashed red line shows the value of the WPTE of an unobstructed link with a separation distance of $L = 0.8$NDR. The used parameters are: $r_a = 50\lambda$, $k_n = k_1$, and NDR $= 6531\lambda$.

Optics EXPRESS

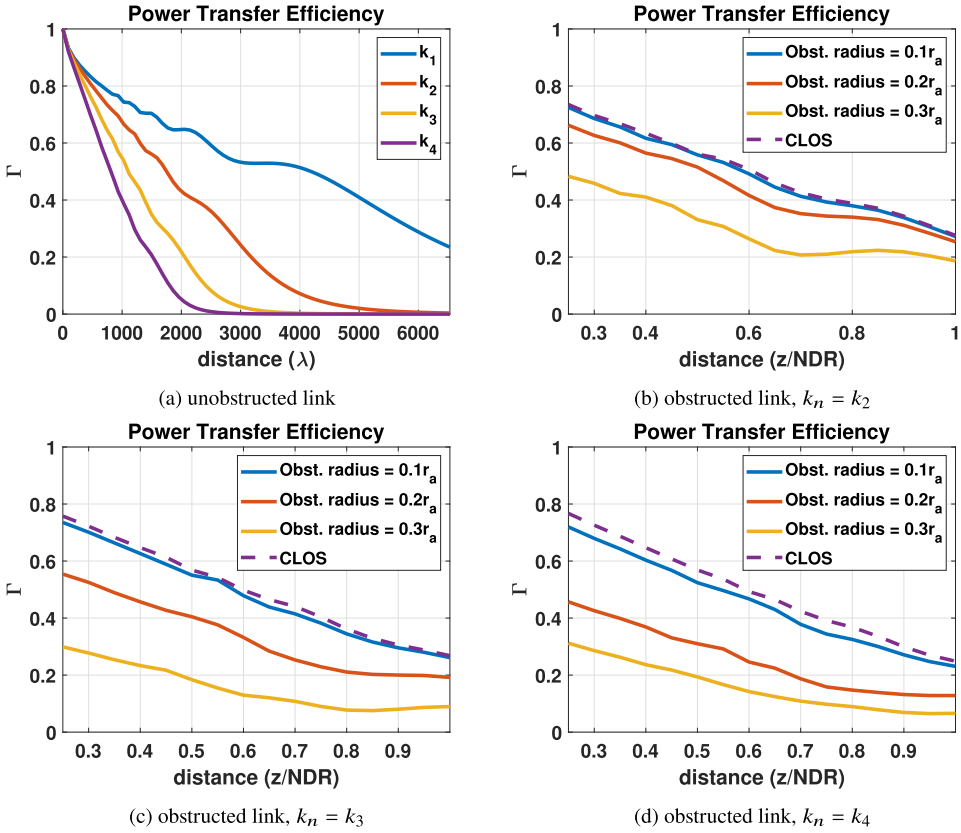

(a) unobstructed link

(b) obstructed link, $k_n = k_2$

(c) obstructed link, $k_n = k_3$

(d) obstructed link, $k_n = k_4$

Fig. 10. WPTE for unobstructed and obstructed links for different k_n. The obstacle is placed at $z = 0.2$NDR. Aperture radius $r_a = 50\lambda$. Figure 10(a) shows the WPTE for unobstructed links. The dashed line represents the WPTE of an unobstructed link

example, the NDR of k_1, k_2, k_3 and k_4 are 6531λ, 2845λ, 1815λ and 1331λ, respectively. As indicated by the larger NDR, we obtain the highest efficiency using k_1. Furthermore, in Fig. 10, we can see that for k_4 the efficiency is disturbed even for obstacles with $r_o = 0.1r_a$. For k_2 and k_3 the smallest obstruction affects the efficiency but it is regenerated to its original value. For the obstacles with $r_o = 0.2r_a$ and $r_o = 0.3r_a$, the efficiency is disturbed and not completely healed when k_n is different than k_1.

4. Conclusion

In this paper, we have studied the wireless power transfer efficiency between two radiating apertures in a wireless link within the Fresnel region. These apertures radiate truncated Bessel beams. In particular, we extended the WPTE formulation to partially obstructed links resorting to a scattering approach. This formulation was implemented using the PO approximation in a variational framework and validated by full-wave results by a commercial software.

It was observed that for distances smaller than the NDR, the WPTE of unobstructed links decrease in an almost linear fashion, while when the system is operating with a separation distance greater than the NDR, the link efficiency decreases quadratically. For the same aperture and separation distance, Bessel beam with small transverse propagation constants provides the highest efficiency.

Optics EXPRESS

Finally, we analyzed the effect of the self-healing property of Bessel beams for obstructed wireless links. The impact of the obstacle on the WPTE was studied considering its position and size. The obtained results illustrate how the size of the obstacle with respect to the radiating aperture radius affect the capability of the Bessel beam to self-heal after an obstruction and thus on the possibility to establish a resilient link. Particularly, for obstacles with radius up to 30% of the aperture radius, the WPTE is fully restored to its unobstructed level. It also appears that Bessel beams with smaller transverse propagation constant can overcome larger obstacles. We saw that WPTE is most affected when the obstacle is located halfway between the apertures and its size is comparable to the radius of the generated beam. Furthermore, the results indicate that the length of the shadow region is not directly related to the WPTE of obstructed links for the studied configuration.

Funding. Agence Nationale de la Recherche (ANR-21-CE25-0014).

Acknowledgments. We acknowledge the collaborators from Institut d'Électronique et des Technologies du numéique (IETR) and Thales Research and Technology.

Disclosures. The authors declare no conflicts of interest.

Data availability. No data were generated or analyzed in the presented research.

References

1. J. Durnin, J. J. Miceli, and J. H. Eberly, "Diffraction-free beams," Phys. Rev. Lett. **58**(15), 1499–1501 (1987).
2. D. McGloin and K. Dholakia, "Bessel beams: Diffraction in a new light," Contemp. Phys. **46**(1), 15–28 (2005).
3. Z. Bouchal, J. Wagner, and M. Chlup, "Self-reconstruction of a distorted nondiffracting beam," Opt. Commun. **151**(4-6), 207–211 (1998).
4. A. Aiello, G. S. Agarwal, and M. Paúr, *et al.*, "Unraveling beam self-healing," Opt. Express **25**(16), 19147–19157 (2017).
5. A. Aiello and G. S. Agarwal, "Wave-optics description of self-healing mechanism in Bessel beams," Opt. Lett. **39**(24), 6819–6822 (2014).
6. X. Chu and W. Wen, "Quantitative description of the self-healing ability of a beam," Opt. Express **22**(6), 6899–6904 (2014).
7. N. Mphuthi, R. Botha, and A. Forbes, "Are bessel beams resilient to aberrations and turbulence?" J. Opt. Soc. Am. A **35**(6), 1021–1027 (2018).
8. A. Trichili, T. Mhlanga, and Y. Ismail, *et al.*, "Detection of Bessel beams with digital axicons," Opt. Express **22**(14), 17553–17560 (2014).
9. B. G. Cai, Y. B. Li, and W. X. Jiang, *et al.*, "Generation of spatial Bessel beams using holographic metasurface," Opt. Express **23**(6), 7593–7601 (2015).
10. M. Ettorre, S. M. Rudolph, and A. Grbic, "Generation of propagating Bessel beams using leaky-wave modes: Experimental validation," IEEE Trans. Antennas Propag. **60**(6), 2645–2653 (2012).
11. G. Mellado-Villaseñor, D. Aguirre-Olivas, and V. Arrizón, "Generation of vector beams using synthetic phase holograms," J. Opt. Soc. Am. A **38**(8), 1094–1103 (2021).
12. J. Baltrukonis, O. Ulcinas, and T. Gertus, *et al.*, "Generation of vector Bessel beams and their application for laser microprocessing of transparent materials," in *2019 Conference on Lasers and Electro-Optics Europe & European Quantum Electronics Conference (CLEO/Europe-EQEC)*, (2019), p. 1.
13. X. Wu, H. Cao, J. Peng, and Z. Meng, "Terahertz quasi non-diffraction bessel vortex beam generation using three lattice types reflective metasurface," Opt. Express **30**(18), 31653–31668 (2022).
14. S. Tu, J. Peng, and Z. Yang, *et al.*, "Single optical element to generate a meter-scale thz diffraction-free beam," Opt. Express **30**(22), 39976–39984 (2022).
15. S. Saltiel, W. Krolikowski, D. Neshev, and Y. S. Kivshar, "Generation of Bessel beams by parametric frequency doubling in annular nonlinear periodic structures," Opt. Express **15**(7), 4132–4138 (2007).
16. Y. Yu and W. Dou, "Generation of pseudo-Bessel beams at thz frequencies by use of binary axicons," Opt. Express **17**(2), 888–893 (2009).
17. S. N. Khonina, N. L. Kazanskiy, S. V. Karpeev, and M. A. Butt, "Bessel beam: Significance and applications-a progressive review," Micromachines **11**(11), 997 (2020).
18. Cisco Systems, "Cisco annual internet report," (2018-2023). [Online; https://www.cisco.com, accessed 27-February-2023].
19. C. Balanis, *Antenna Theory: Analysis and Design*, Jeff borrow list (John Wiley & Sons, 2005).
20. M. Ettorre and A. Grbic, "Generation of propagating Bessel beams using leaky-wave modes," IEEE Trans. Antennas Propag. **60**(8), 3605–3613 (2012).
21. R. C. M. Pimenta, G. Soriano, and K. D. Paschaloudis, *et al.*, "Self-healing analysis of distorted weakly-diffracting vector beams," in *2023 17th European Conference on Antennas and Propagation (EuCAP)*, (2023), pp. 1–3.

Optics EXPRESS

22. F. Alsolamy, W. A. Alomar, and A. Grbic, "Cylindrical vector beams for wireless power transfer," IEEE Trans. Antennas Propag. **69**(3), 1716–1727 (2021).
23. C. Balanis, *Advanced Engineering Electromagnetics*, 2nd Edition (Wiley, 2012).
24. S. Pakovic, S. Zhou, and D. González-Ovejero, *et al.*, "Bessel-Gauss beam launchers for wireless power transfer," IEEE Open J. Antennas Propag. **2**, 654–663 (2021).
25. J. D. Heebl, M. Ettorre, and A. Grbic, "Wireless power transfer with Bessel beams," in *2016 10th European Conference on Antennas and Propagation (EuCAP)*, (2016), pp. 1–2.
26. F. Benassi, W. Fuscaldo, and D. Masotti, *et al.*, "Wireless power transfer in the radiative near-field through resonant Bessel-beam launchers at millimeter waves," in *2021 IEEE Wireless Power Transfer Conference (WPTC)*, (2021), pp. 1–4.
27. M.-K. Hu, "Near-zone power transmission formula," IRE Nat'l Conv. Rec. **6**, 128–135 (1958).
28. G. V. Borgiotti, "Maximum power transfer between two planar apertures in the fresnel zone," IEEE Trans. Antennas Propag. **14**(2), 158–163 (1966).
29. R. F. Harrington, *Time-Harmonic Electromagnetic Fields* (Wiley-IEEE, 2001).
30. V. Rumsey, "Reaction concept in electromagnetic theory," Phys. Rev. **94**(6), 1483–1491 (1954).
31. N. Marcuvitz, I. of Electrical Engineers and M. I. of Technology. Radiation Laboratory, Waveguide Handbook, *IEE electromagnetic waves series* (McGraw-Hill, 1951).
32. J. Goodman, *Introduction to Fourier Optics*, McGraw-Hill physical and quantum electronics series (W. H. Freeman, 2005).
33. R. F. Harrington, "On scattering by large conducting bodies," IRE Trans. Antennas Propag. **7**(2), 150–153 (1959).
34. R. F. Harrington, *Field Computation by Moment Methods*, Macmillan Series in Electrical Science (R.E. Krieger Publishing Company, 1982).
35. W. Gibson, *The Method of Moments in Electromagnetics* (CRC, Taylor & Francis Group, 2021).
36. K. Milton and J. Schwinger, *Electromagnetic Radiation: Variational Methods, Waveguides and Accelerators* (Springer Berlin Heidelberg, 2006).
37. COMSOL AB, "Comsol multiphysics," https://www.comsol.com (2023).